

# Drag Characteristics of a Low-Drag Low-Boom Supersonic Formation Flying Concept

Yuichiro Goto\* , Shigeru Obayashi† and Yasuaki Kohama‡

*Tohoku University, Sendai, Japan*

In this paper, a new concept for low-drag, low-boom supersonic flight, by formation flying is proposed. This concept takes advantage of the shock wave and expansion wave interactions among the aircrafts in the fleet. Drag characteristics analysis is carried out on the concept to validate the effectiveness of supersonic formation flying as a means to reduce the wave drag of the fleet of supersonic aircrafts. Analysis results indicate promising drag reduction for supersonic formation flying, and insight on the physics of wave interactions in formation flying is obtained.

## Nomenclature

$M$	Freestream Mach number
$\beta$	$\sqrt{M^2 - 1}$
$\mu$	Mach angle
$C_L$	Lift coefficient
$C_{D_s}$	Drag coefficient of the SST
$C_{D_e}$	Drag coefficient of the elliptic wing
$C_{D_{i_s}}$	Induced drag coefficient of the SST
$C_{D_{i_e}}$	Induced drag coefficient of the elliptic wing
$C_{D_{cvol_s}}$	Volume wave drag coefficient of the SST
$C_{D_{cvol_e}}$	Volume wave drag coefficient of the elliptic wing
$C_{D_{clift_s}}$	Lift dependent wave drag coefficient of the SST
$C_{D_{clift_e}}$	Lift dependent wave drag coefficient of the elliptic wing
$AR_s$	Aspect ratio of the SST
$AR_e$	Aspect ratio of the elliptic wing
$b_s$	Span of the SST
$b_e$	Span of the elliptical wing
$c_s$	Root chord length of the SST
$c_e$	Root chord length of the elliptical wing
$t_s$	Maximum thickness of the SST
$t_e$	Maximum thickness of the elliptical wing
$S_s$	Wing area of the SST
$S_e$	Wing area of the elliptical wing
$r_s$	Maximum fuselage cross-section radius of the SST
$L_s$	Fuselage length of the SST
$e$	Span efficiency factor of the SST
$r, \theta, x_{myu}$	Three parameters for new coordinate system

\*Graduate Student, Department of Aeronautics and Space Engineering. Student Member AIAA.

†Professor, Institute of Fluid Science. Associate Fellow AIAA.

‡Professor, Institute of Fluid Science.

## I. Introduction

In the past 50 years, although the technology for transonic flight has matured, commercially practical civil supersonic transport has not been realized. The two major problems that have prevented supersonic commercial transportation are wave drag and sonic boom.

Wave drag, which is the dominating component of drag at supersonic speeds, leads to a deterioration in cruise efficiency. And sonic booms have a problem of public acceptance, which gives supersonic transports strict limitations on overland flight. This leads to less flexible operation capabilities, reducing its profitability.

Many attempts have been made to minimize the wave drag and the sonic boom in the past. Among them, many studies approached this problem by optimizing the shape of the wing body configuration. However, most studies have shown a strong trade-off between wave drag and sonic boom, making it impossible to minimize wave drag and sonic boom simultaneously, for a given aircraft overall length.

The supersonic formation flying concept proposed in this paper, utilizes wave interference for the reduction of wave drag and sonic boom. For the reduction of wave drag, favorable wave interference is used for the following aircraft to extract momentum from the pressure gradients in the flow field behind the leading aircraft. And the reduction in the loudness of the sonic boom is achieved by a virtual elongation effect of the aircraft overall length, obtained from wave interference.

In this paper, drag characteristics of this concept is investigated using Euler simulations. The dependence of wave drag to the relative position of the aircraft is investigated to evaluate the effectiveness of this concept and gain insight on the drag characteristics of supersonic formation flying.

## II. Concept

The supersonic formation flying concept proposed here utilizes the benefits of multi-body favorable wave interference to reduce the volume and lift dependent wave drag of the following aircraft. When an aircraft flies through the air at supersonic speeds, they leave momentum in the air behind them. This is the cause of wave drag. Wave drag of the following aircraft is reduced by collecting this momentum as pressure gradient.

Friedman et al<sup>1</sup> carried out linear analyses on bodies of revolution, imitating a fuselage and stores. As a result they have shown that wave drag per total cross-sectional area can be reduced when placed in an optimal relative position. Positions of the stores that were favorable for wave drag reduction were positions where the stores were placed inside a shock wave, which is a positive pressure jump.

The reduction of sonic boom of the fleet will be achieved by virtually elongating the aircraft. Marconi et al.<sup>2</sup> showed that, instead of simple elongation of the aircraft overall length, off-axis volume addition is also effective for boom mitigation. Volume was added by placing a small keel-like forward-swept wing at the nose of the aircraft. As a result, they succeeded in reducing the amount of extension to the fuselage by a factor of  $\tan \mu$ . In the concept proposed in this paper, a similar idea is applied to a fleet of aircrafts to reduce the sonic boom.

It is a well known fact that the pressure signature of the sonic boom is dependent on the overall length and the area distribution of the aircraft  $A(x)$ . This area distribution is defined by a sweep of a plane inclined downward at the Mach angle. If aircrafts are placed in a way such that the nose of the following aircrafts is in front of this inclined plane extending from the tail of the preceding aircraft, the area distribution of the aircraft will be clustered together, resulting in a longer duration time for the pressure wave profile. This results in the reduction in the loudness of the sonic boom perceived on the ground. A sketch of this idea is shown in Fig.1.

Bahm et al.<sup>3</sup> carried out some flight tests to measure the ground recorded sonic boom produced by a formation of two F-18s. In the re-

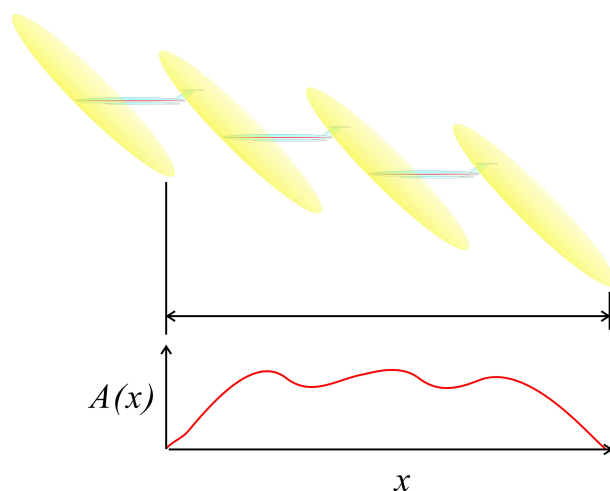


Figure 1. Sketch of area distribution continuation

sults of this preliminary flight tests, it was possible to fly two aircrafts, which originally produces an N wave on the ground, and produce flattop type signatures by flying in formations.

### III. Computational Method

Euler simulations are carried out using *TAS-flow*, an unstructured Euler/Navier-Stokes solver, and the computational mesh was generated using *EdgeEditor* and *TU TetraGrid*, which are CFD tools developed at Tohoku University.

*TAS-flow* is an unstructured Euler/Navier-Stokes solver using a finite-volume cell-vertex scheme, HLLW Riemann solver for flux computations,<sup>4</sup> and LU-SGS implicit scheme for time integration.<sup>5</sup> *EdgeEditor* is an unstructured surface mesh generation software. It takes CAD data as an input,<sup>6</sup> and generates a surface mesh using an advancing front triangulation method.<sup>7</sup> *TU TetraGrid* is an unstructured volume mesh generation software using the Delaunay triangulation algorithm.<sup>8</sup>

As for the coordinate system used in this analysis,  $x$  is in the freestream direction,  $y$  is out towards the right wing tip, and  $z$  is upward. The origin of the coordinate system is located at the half chord position along the centerline of the leading aircraft. The freestream Mach number used in this analysis is  $M = 1.5$ . This Mach number was chosen considering recent trends in the cruise Mach number of recent supersonic transports concepts.

Since the objective of this study is to investigate the effectiveness of supersonic formation flying, the subject of the analysis is kept simple to extract the effect of shock wave interaction alone, and facilitate the analysis. First of all, simulations are carried out on two aircraft formations. And, the model used for this study is an elliptical planform wing with a biconvex airfoil.

Although simplification of the configuration is convenient, the drag characteristic of the simplified model must be similar to that of a practical supersonic transport. The aspect ratio and thickness are determined to satisfy this condition.

First, the practical supersonic transport model is approximated as a wing-body configuration consisting of an ellipsoidal wing and a Sears-Haack body of revolution as the fuselage. The drag of the components are estimated using the following equations,<sup>9</sup>

$$C_{D_s} = C_{Di_s} + C_{Dc\ vol_s} + C_{Dc\ lift_s} \quad (1)$$

where each drag component is given by,

$$C_{Di_s} = \frac{C_L^2}{\pi A R_s e} \quad (2)$$

$$C_{Dc\ vol_s} = \frac{4\pi^2 r_s^2 \pi r_s^2}{L_s^2 S_s} + \left[ \frac{\beta^2 + 2(c_s/b_s)}{\beta^2 + (c_s/b_s)} \right] \frac{t_s^2}{c_s^2} \quad (3)$$

$$C_{Dc\ lift_s} = \frac{\beta^2 C_L^2}{2 \pi c_s} \quad (4)$$

This drag model is compared with that of a single elliptical wing, expressed in the following form,

$$C_{D_e} = C_{Di_e} + C_{Dc\ vol_e} + C_{Dc\ lift_e} \quad (5)$$

where each drag component is given by,

$$C_{Di_e} = \frac{C_L^2}{\pi A R_e} \quad (6)$$

$$C_{Dc\ vol_e} = \left[ \frac{\beta^2 + 2(c_e/b_e)}{\beta^2 + (c_e/b_e)} \right] \frac{t_e^2}{c_e^2} \quad (7)$$

$$C_{Dc\ lift_e} = \frac{\beta^2 C_L^2}{2 \pi c_e} \quad (8)$$

The numbers for the drag model are given below. Most values for the SST drag model are taken from

the Concorde.<sup>10</sup>

$$AR_s e = 1.5 = \frac{b_s^2}{\pi b_s/2 c_s/2} \quad (9)$$

$$b_s/c_s = 1.5\pi/4 \quad (10)$$

$$t_s/c_s = 0.04 \quad (11)$$

$$r_s/L_s = 0.0234 \quad (12)$$

These values are substituted into the drag model, and the drag models are compared to solve for the aspect ratio and the thickness of the simplified elliptic wing. This resulted in an elliptic wing with the following dimensions.

$$AR_e = 1.5$$

$$b_e/c_e = 1.5\pi/4$$

$$t_e/c_e = 0.04502$$

$$S_e = 0.9253$$

A three view diagram of this configuration is given in Fig.2.

In this paper, the angle of attack of the wings are maintained at  $\alpha = 3.25^\circ$ . And the drag characteristics are evaluated by comparing the changes in both the  $C_L$  and  $C_D$  of the wings. This angle of attack was chosen so that the  $C_L$  of the leading wing which is flying in undisturbed freestream equals 0.146.

The mesh used in this analysis is an unstructured full three-dimensional mesh with 1.05 million grid points, and 21,000 grid points on each wing. The symmetry plane of this mesh is given in Fig.3. A full three dimensional mesh is used to allow for asymmetric formations. Grid convergence of the aerodynamic coefficients of the leading aircraft has been checked on several grids. The standard deviation of the  $C_D$  of the following wing was 0.15 counts for the data shown in this paper.

## IV. Results

The relative position and aerodynamic performance of the following aircraft in the 63 investigated formations are shown in Table 1. The coordinates are normalized by the chord length.

The best  $L/D$  of the Following aircraft was achieved in *Case 51*. The following aircraft in this formation achieved a 31.4% improvement in  $L/D$ . The lift and drag coefficients of the following aircraft in this formation was  $C_L = 0.14181$  and  $C_D = 0.01367$ . These values indicate that the improvement in  $L/D$  is achieved by reducing the drag while maintaining the lift. The  $C_p$  contour on the  $y = 0$  plane is shown in Fig.4. In this formation, the leading edge of the following aircraft is placed in the expansion wave of the leading aircraft.

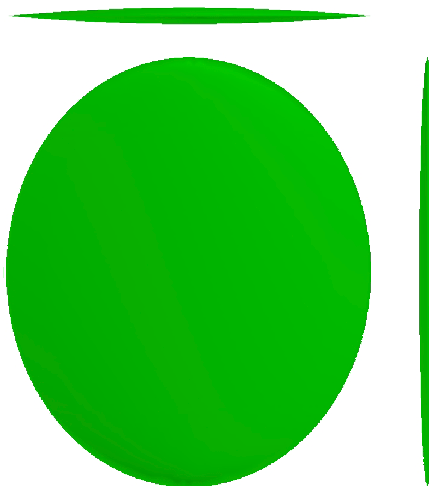


Figure 2. Three view diagram of simplified model

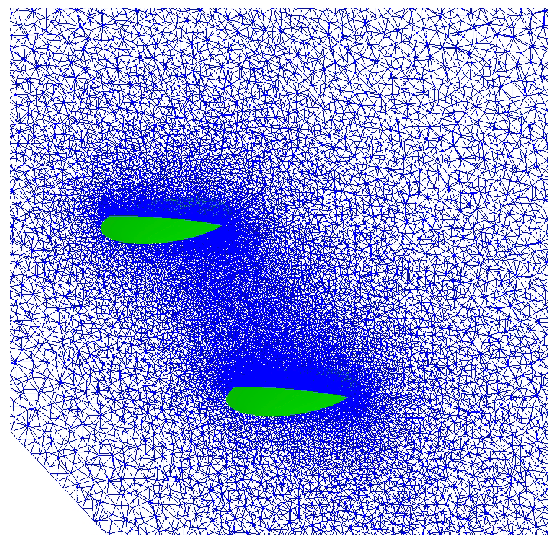


Figure 3. Symmetry plane of computational mesh

To investigate the cause of this improvement in aerodynamic performance, the chord wise  $C_p$  distribution of the aircrafts are shown in Fig. 5. In this figure, the root  $C_p$  distribution of the following aircraft is plotted over that of the leading aircraft. Here, the reduction in  $C_p$  near the leading edge of the following aircraft is due to the impinging of the expansion wave extending from the leading aircraft. This resulted in the dramatic reduction in drag of the following aircraft. Near the mid-chord position of the following aircraft, there is a pressure peak due to the impinging of the shock wave extending from the trailing edge of the leading aircraft. This peak in  $C_p$  acts to compensate for the loss in lift caused by the impinging of the expansion wave.

On the other hand, the worst  $L/D$  was achieved in *Case 1*. The following aircraft, in this formation, experienced a 41.0% reduction in  $L/D$ . The lift and drag coefficients of the following aircraft were  $C_L = 0.07111$  and  $0.01526$ . Even though there was a considerable reduction in the drag of the following aircraft, this was not enough to compensate for the extensive reduction in lift. The  $C_p$  contour at the  $y = 0$  plane is shown in Fig.6. In this formation, the shock wave extending from the leading edge of the leading aircraft impinges on the upper surface of the following aircraft, leading to a reduction in lift.

To visualize the effect of the impinging shock wave more qualitatively, root  $C_p$  distributions are compared in Fig.7. The  $C_p$  distribution of the following aircraft indicates that almost the whole upper surface of the following aircraft is being spoiled by the shock wave and the high pressure region extending from the leading aircraft, reducing the lift dramatically. But, the high pressure acting on the downstream half of the upper surface acts to reduce the wave drag acting on the aircraft, although this benefit is not enough to compensate for the loss in lift.

Since the current supersonic formation flying concept also aims to reduce the sonic boom, the shock waves propagating downward towards the ground must interact with the following aircraft aircraft. Therefore, formations where the following aircraft is placed below the leading aircraft, are thought to be more effective in reducing the sonic boom. Such a formation that achieved the best value of  $L/D$  was *Case 3*. Here, the following aircraft achieved a 16.9% improvement in  $L/D$ , at  $C_L = 0.15884$  and  $C_D = 0.01721$ . The  $C_p$  contour of the  $y = 0$  plane is shown in Fig.8. Here, the leading edge of the following aircraft is inside the expansion fan of the leading aircraft. This contributes to the reduction in drag and the increase in lift.  $C_p$  distribution is shown in Fig.9. This shows that the shock wave extending from the trailing edge of the leading aircraft impinges on the upper surface. As a result, the upstream half of the aircraft is exposed to low pressure and the downstream half of the aircraft is exposed to high pressure, giving the aircraft additional thrust.

To investigate how the relative position affects the aerodynamic performance of the following aircraft, a subset of the data set is examined.

Here, *Cases 1 to 8* are examined. The formation with the largest values of  $L/D$  are *Case 3* and *Case 7*. In these formations, the coordinates of the following aircraft are  $(2.0, 0.0, -1.34)$  and  $(2.5, 0.0, 1.79)$  respectively, the values of  $C_L$  are  $0.15884$  and  $0.16161$ , the values of  $C_D$  are  $0.01721$  and  $0.01761$ , and finally, the values

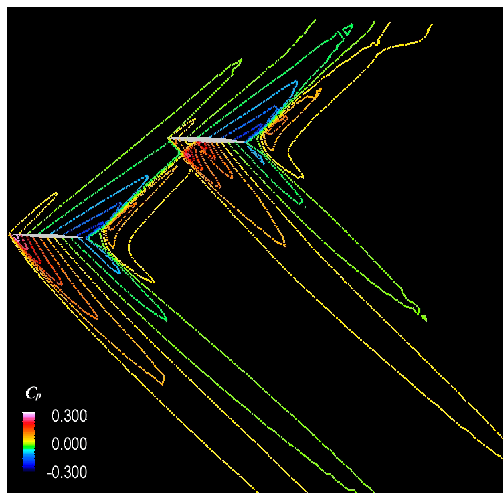


Figure 4.  $C_p$  contour of symmetric plane, *Case 51*

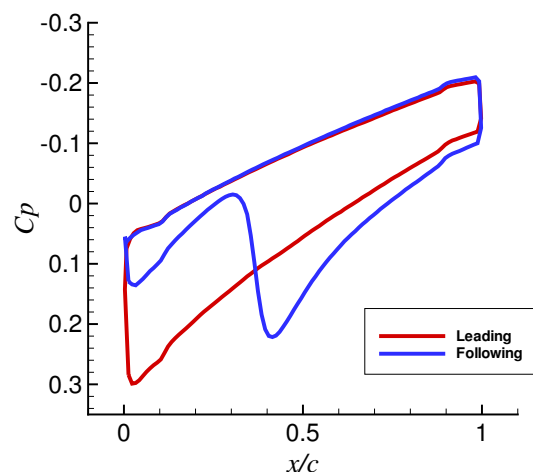


Figure 5.  $C_p$  distribution, *Case 51*

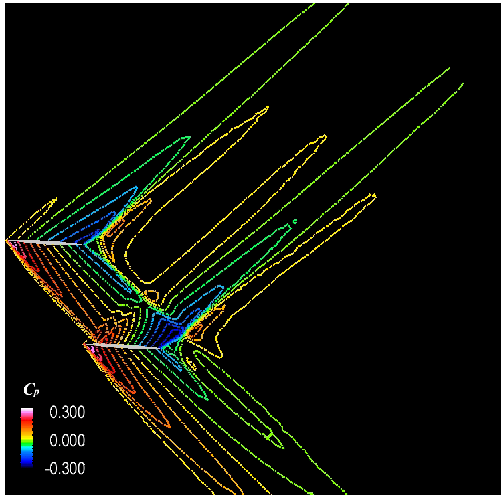


Figure 6.  $C_p$  contour of symmetric plane, Case 1

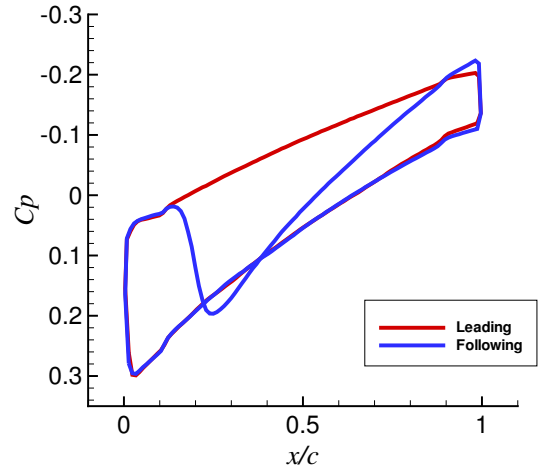


Figure 7.  $C_p$  distribution, Case 1

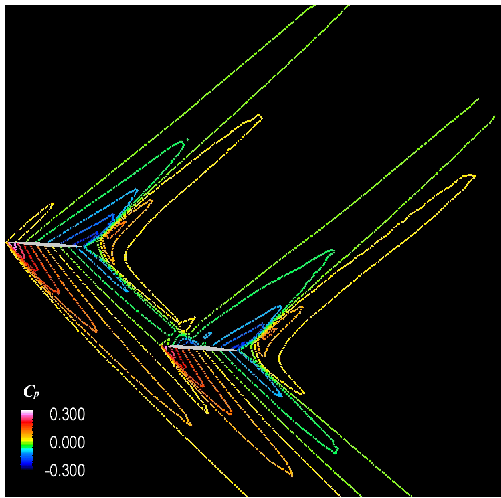


Figure 8.  $C_p$  contour of symmetric plane, Case 3

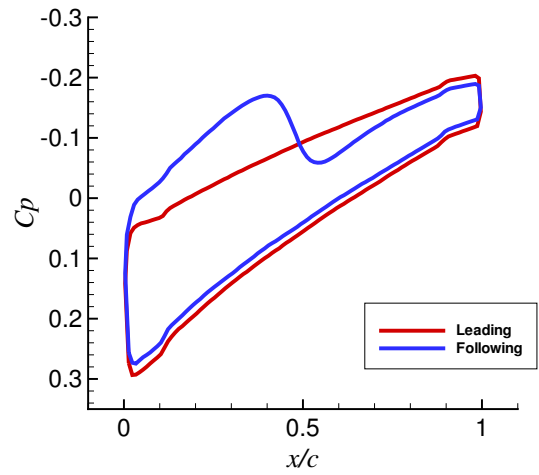


Figure 9.  $C_p$  distribution, Case 3

of  $L/D$  are 9.23 and 9.18. Comparing the two cases, it is obvious that aerodynamic performance of these two cases are very similar. Both formation achieves a high  $L/D$  by increasing the lift instead of reducing the lift, and the amount of increase in lift is also similar. The  $C_p$  distribution of the following aircraft for these two cases are compared in Fig.10. Comparing the  $C_p$  distributions, they can be almost identical, including the position of the impinging shock wave. The only difference between the two is the fact that in Case 7, which is the case where the following aircraft is placed further away from the leading aircraft, the shock wave is dissipated, and the pressure gradient slope due to the impinging shock is shallower.

The formations with the smallest values of  $L/D$  are Case 1 and Case 5. In these formations, the coordinates of the following aircraft are  $(1.0, 0.0, -1.34)$  and  $(1.5, 0.0, 1.79)$  respectively, the values of  $C_L$  are 0.07111 and 0.08472, the values of  $C_D$  are 0.01526 and 0.01672, and finally, the values of  $L/D$  are 4.66 and 5.07. Similar trends can be seen in these two formations as well. The poor performance is caused by a dramatic loss of lift in both cases. The  $C_p$  distribution of the following aircraft for these two cases are compared in Fig.11. Again, in comparing the  $C_p$  distributions for the two cases, the only difference is a difference in the impinging position of the shock wave, and the dissipation of the shock wave.

In this subset of the data set, similar results are obtained for pairs of cases where the difference in the positions of the following aircrafts are  $\Delta x = 0.5$ ,  $\Delta y = 0.0$ ,  $\Delta z = 0.45$ . This corresponds to the two following aircrafts being on the same Mach line extending downstream from the leading aircraft. Similar results are obtained in these cases because the Mach lines are what characterizes the flow field in supersonic

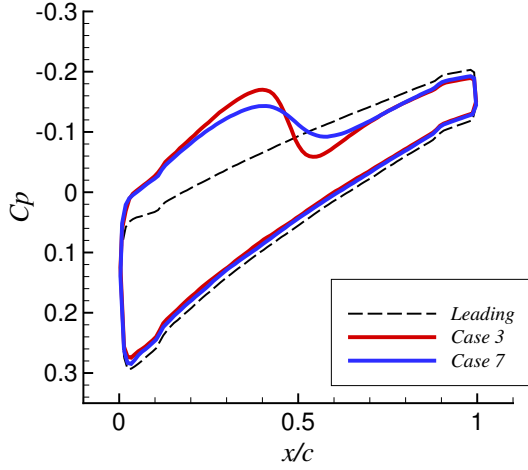


Figure 10. Comparison of the  $C_p$  distribution of the following aircrafts, Case 3 and Case 7

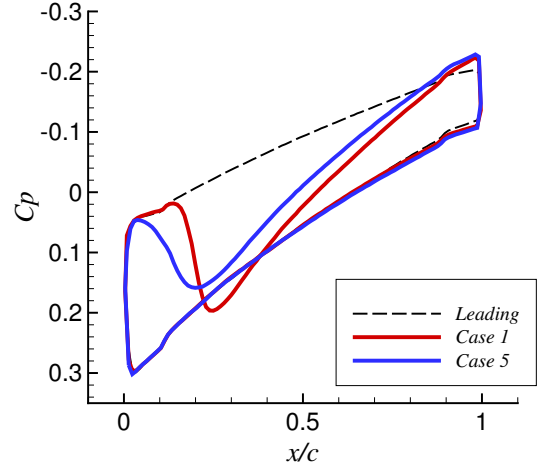


Figure 11. Comparison of the  $C_p$  distribution of the following aircrafts, Case 1 and Case 5

flow and there exists very similar flow conditions along a Mach line.

Same analyses have been carried out on other subsets of the data set, and following aircrafts existing on the same Mach line showed similar aerodynamic performance for most Mach lines.

## V. Discussions

### A. Dependence of Wave Drag on Relative Position

From the results above, it is obvious that the interaction between the following aircraft and the shock and expansion waves extending from the leading aircraft is an important factor in the modification of aerodynamic performance.

To understand the dependence of wave drag on relative position more effectively, a new coordinate system, which takes into account the physics of the wave interaction, is introduced. In the new coordinate system, the position of the following aircraft is expressed using three parameters  $r$ ,  $\theta$  and  $x_\mu$ . The conversion between the conventional Cartesian coordinate system and the new coordinate system is given by the following equations.

$$r = \sqrt{y^2 + z^2} \quad (13)$$

$$\theta = \arg(-z + yi) \quad (14)$$

$$x_\mu = x - r/\tan \mu \quad (15)$$

First of all,  $r$  is a parameter to express how far away along the Mach cone, the following aircraft is located from of the leading aircraft. To make the coordinate system intuitive,  $r$  is defined as the distance between the longitudinal axes of the leading and following aircrafts. Next,  $\theta$  is the azimuthal position in the  $yz$  plane. Here,  $\theta$  is defined so that, if  $\theta = 0^\circ$ , then the following wing is placed below the leading aircraft, and if  $\theta = 90^\circ$ , following wing is placed to the portside of the leading aircraft. And finally,  $x_\mu$  expresses the streamwise position of the following aircraft with respect to the Mach cone extending downstream from the center of the leading aircraft. Although there are small discrepancies due to nonlinearity,  $x_\mu$  can be regarded as a parameter that indicates how the following wing interacts with the shock and expansion waves. More specifically, if  $x_\mu \approx -0.5$ , then the upstream half of the following wing will be in undisturbed freestream and the leading edge shock of the leading aircraft will be impinging near the mid chord point of the following aircraft, and if  $x_\mu \approx 0.0$ , the leading edge shock of the leading aircraft will be impinging near the leading edge of the following aircraft, and so on.

Figure 12 is a diagram showing the relation between the conventional Cartesian coordinate system and the new coordinate system. In this figure, the conventional coordinate system is drawn in black dashed lines, the Mach cone is drawn in orange lines, and the definition of the new coordinate system is drawn in green lines.

Aerodynamic performance of the 63 formations are analyzed using the new coordinate system.

First of all, aerodynamic performance values are compared against  $x_\mu$ . Results are shown in figs. 13 to 15.

In these figures, different symbols correspond to data set with different values of  $\theta$ , and the aerodynamic performance of the leading aircraft is shown as a dashed line. Organized in the coordinate system, the data points of most of the data sets form a fairly smooth single curve. This shows that the aerodynamic performance of the following aircraft shows good correlation with the parameter  $x_\mu$ .

First, formations where  $\theta = 0^\circ$  are investigated. In this case, the following aircraft is placed under the leading aircraft. Looking at  $C_L$ , it has a peak near  $x_\mu = 0.1$ , and the performance deteriorates as values of  $x_\mu$  get larger or smaller. This is due to the fact that the benefit

of interaction with the expansion wave is greatest near this peak, and the effect of shock waves extending

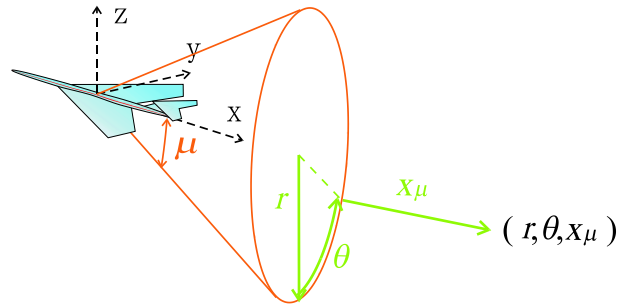


Figure 12. Definition of the new coordinate system

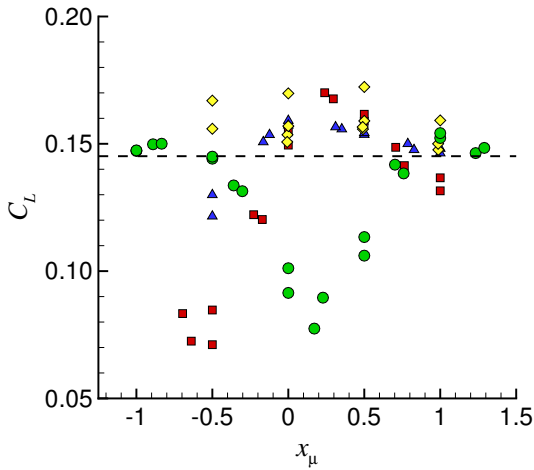


Figure 13.  $C_L$  for all formations

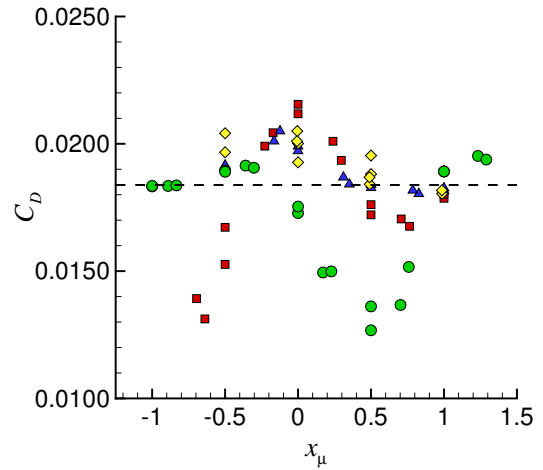


Figure 14.  $C_D$  for all formations

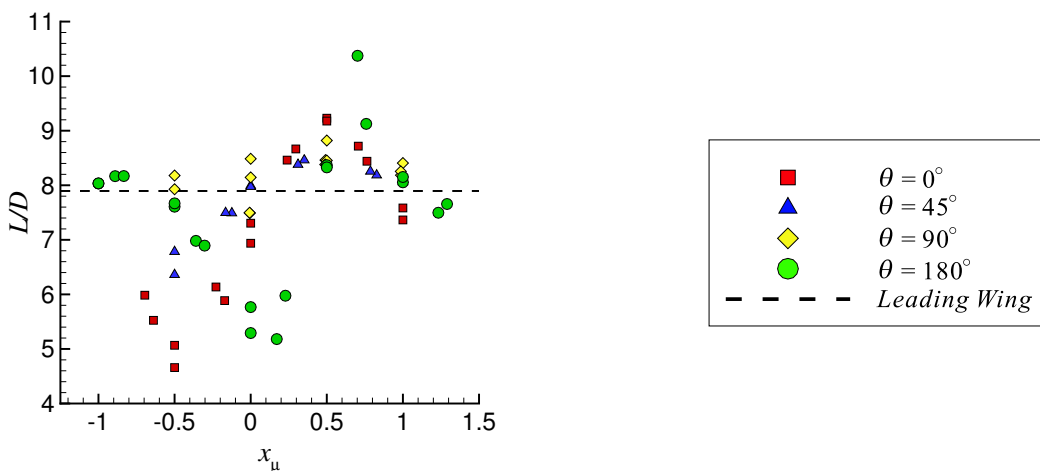


Figure 15.  $L/D$  for all formations

from leading and trailing edges of the leading aircraft take effect when  $x_\mu$  moves off this value. Worst performance in  $C_L$  is seen near  $x_\mu = -0.6$ . This is due to the fact that if the following aircraft is placed too far forward, it stops interacting with the expansion wave, and stops receiving the benefits from the suction, while the impinging shock wave spoils its lift.  $C_D$  also has a maximum near  $x_\mu = 0.0$ . This is the position where the high pressure after the shock acts on the upstream half of the following aircraft, and the expansion fan impinges on the downstream half. Since the following aircraft exists inside this negative pressure gradient, the drag increases. When the following aircraft starts interacting with the leading edge or the trailing edge shock of the leading aircraft, it will be inside a positive pressure gradient, and the momentum in this pressure gradient is recovered as thrust. Looking at  $C_L$ , the most favorable position is near  $x_\mu = 0.1$ , and if  $C_D$  is considered, performance improves as  $x_\mu$  moves away from 0.0. Therefore, as seen in fig.15, the best values for  $L/D$  exist near  $x_\mu = 0.5$ .

Next, formations where  $\theta = 180^\circ$  are investigated. In this case, the following aircraft is placed above the leading aircraft. Here,  $C_L$  performance depicts an opposite trend compared to the previous case. The interaction with the shock waves, occurring at larger or smaller values of  $x_\mu$ , maintains the value of  $C_L$  to be close to that of the leading aircraft, but interactions with the expansion wave reduces the  $C_L$  by about 40%. As for the value of  $C_D$ , the trend is very similar to the drag characteristics of formations with  $\theta = 0^\circ$ , if the difference in lift dependent shock or expansion wave is taken into account. Since, in this case, the expansion fan is larger in range and strength, the benefits of drag reduction is much greater. Maximum value of  $L/D$  is obtained near  $x_\mu = 0.70$ .

In the two cases above, the sensitivity of aerodynamic performance to  $x_\mu$  is evaluated. Looking at the  $C_L$  and  $C_D$  plots in the region where the formations achieved best  $L/D$ , in both cases, the  $C_L$  and  $C_D$  plots have a very steep slope. This indicating that these aerodynamic coefficients are changing drastically in this region. This may cause controls problems when in actual flight. Position keeping in cruise may need active automatic controlling and also, transitioning into this formation may be even more difficult.

In cases where  $\theta = 45^\circ$  and  $90^\circ$ , improvements and deteriorations, from the performance of the leading aircraft, is smaller than in previous cases. Looking at the  $C_p$  contour plots of the flow field behind the leading aircraft, shock and expansion waves propagating in the vertical direction were stronger than that propagating in the horizontal direction. Therefore, more momentum propagates in the vertical plane, and the amount of momentum in the air that the following aircraft can carry becomes less as the following aircraft moves off the  $y = 0$  plane. But, on the other hand, aircraft handling characteristics for the following aircraft will improve, as the effect of wave interaction becomes moderate.

Next, aerodynamic performance is plotted against  $r$ , in figs.16 to 18, to investigate the dependence on the distance between the two aircrafts. Here, it can be seen that, as the distance between the two aircrafts increase, the data points moves closer towards the values of the leading aircraft. This indicates that the effect of wave interaction becomes weaker as the distance between the aircrafts increase. This reduces the benefits of wave interaction, but on the other hand, may result in more moderate aircraft characteristics.

## B. Constant Lift Analysis

In the current study, all analyses have been carried out at a constant angle of attack. But aircraft, in straight and level cruise, must generate exactly the amount of lift that balances the weight of aircraft, and consequently, will have to fly at constant  $C_L$ .

In linear analysis of the lift dependent wave drag, it is known that,<sup>11</sup>

$$C_D \propto \alpha^2 \quad (16)$$

$$C_L \propto \alpha \quad (17)$$

which means that an increase in  $C_L$  is more valuable compared to a reduction in  $C_D$ . This indicates a need to consider cases with similar values of  $L/D$ , which are cases where the high  $L/D$  is achieved by an increase in lift instead of a reduction in drag.

Here, we consider *Case 36*, where the amount of produced lift is highest. The original aerodynamic coefficients were,  $C_L = 0.16766$ ,  $C_D = 0.01935$ , which results in an  $L/D$  of 8.66. This formation was recalculated so that the  $C_L$  of the following wing becomes approximately 0.1. The result of the recalculation was,  $C_L = 0.145823$ ,  $C_D = 0.01565$ , which corresponds to  $L/D = 9.31$ .

Therefore, a constant lift analysis is important for a precise evaluation of performance.

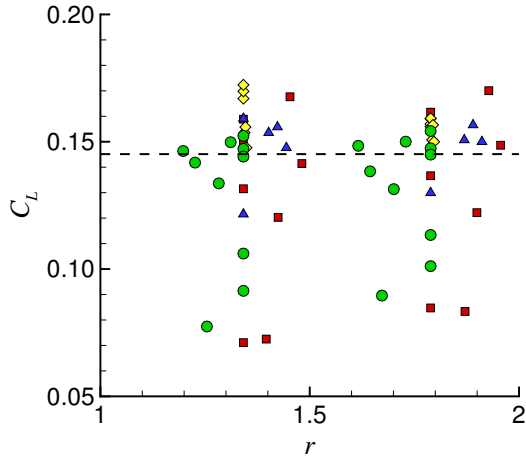


Figure 16.  $C_L$  for all formations

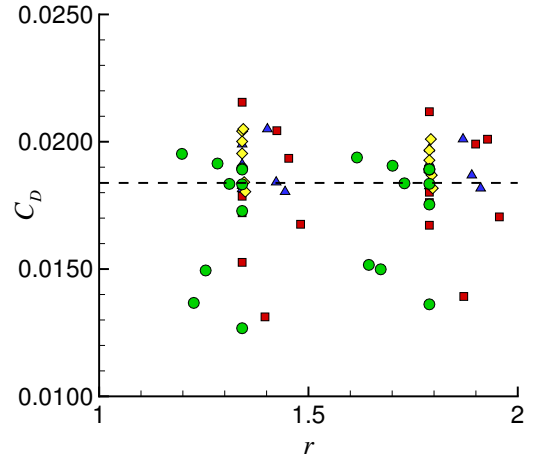


Figure 17.  $C_D$  for all formations

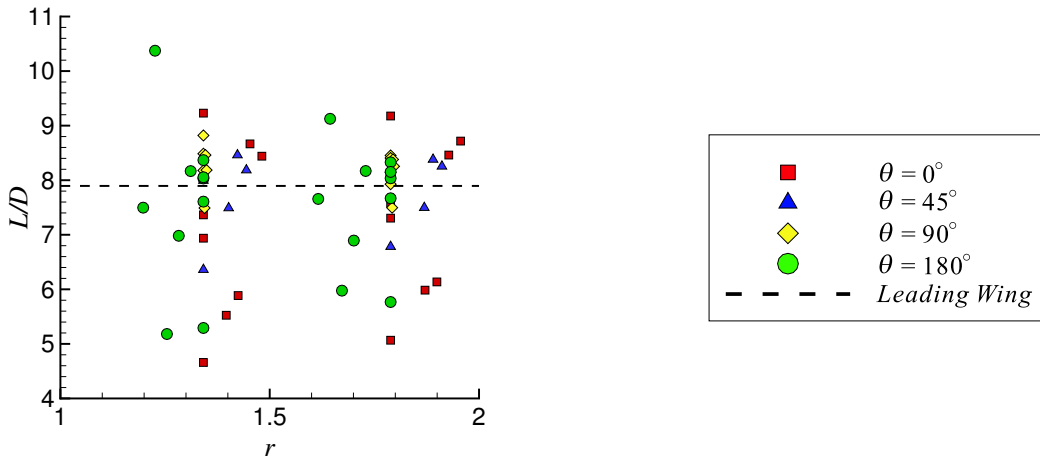


Figure 18.  $L/D$  for all formations

## VI. Conclusions

In this study, a new concept to achieve low-drag and low-boom by formation flying of supersonic transports has been proposed. This concept takes advantage of the shock wave and expansion wave interaction to reduce the total drag and boom of a fleet of supersonic transports.

The investigation of drag characteristics for different arrangements of the formation has also been carried out. From these results, it can be concluded that the supersonic formation flying concept showed up to 30% increase in  $L/D$  and therefore deserves further research as a means to reduce the wave drag of a fleet of supersonic aircrafts. The best  $L/D$  values were achieved when the following aircraft interacts with the expansion wave of the leading aircraft.

To organize the data, taking into account the physics of the drag reduction mechanism, a new coordinate system, which are made up of parameters that indicate the degree of interaction with the shock and expansion waves, has been introduced. This coordinate system has been proven to be very effective in extracting the physics in the wave interference. In this coordinate system, the physics of interaction with shock and expansion waves is dominated by  $x_\mu$ , and the effect of diffusion of the shock and expansion waves is expressed by  $r$ .

Finally, short-term goals for future work include evaluation of formations under  $C_L$  constraints, and optimization of the fleet of aircraft. Long-term goals include evaluation of sonic boom, and multi-objective optimization of the arrangement of the formation for minimization of wave drag and sonic boom.

## VII. Acknowledgments

This research has been funded by the Leading Researcher Hatchery Program from the 21st Century COE, Flow Dynamics International Research Educational Base, at the Institute of Fluid Science, Tohoku University. Authors would also like to thank Prof. K. Nakahashi and the Spacecraft Systems Laboratory, Department of Aerospace Engineering, Tohoku University for providing the CFD analysis tools.

## References

- <sup>1</sup>Friedman, M. D. and Cohen, D., "Arrangement of Fusiform Bodies to Reduce the Wave Drag at Supersonic Speeds," *NACA Report*, 1236, 1955.
- <sup>2</sup>Marconi, F., Bowersox, R., Orr, M., Mozingo, J., and Schetz, J., "Sonic Boom Alleviation using Keel Configurations," *AIAA Paper*, 2002-0149, 2002.
- <sup>3</sup>Bahn, C. M. and Haering, Jr., E. A., "Ground-Recorded Sonic Boom Signatures of F-18 Aircraft in Formation Flight," 1995.
- <sup>4</sup>Obayashi, S. and Guruswamy, G. P., "Convergence Acceleration of an Aeroelastic Navier-Stokes Solver," *AIAA Journal*, Vol. 33, No. 6, 1994, pp. 1134–1141.
- <sup>5</sup>Sharov, D. and Nakahashi, K., "Reordering of Hybrid Unstructured Grids for Lower-Upper Symmetric Gauss-Seidel Computations," *AIAA Journal*, Vol. 36, No. 3, 1998, pp. 484–486.
- <sup>6</sup>Ito, Y. and Nakahashi, K., "Surface Triangulation for Polygonal Models Based on CAD Data," *International Journal for Numerical Methods in Fluids*, Vol. 39, Issue 1, 2002, pp. 75–96.
- <sup>7</sup>Ito, Y. and Nakahashi, K., "Direct Surface Triangulation Using Stereolithography Data," *AIAA Journal*, Vol. 40, No. 3, 2002, pp. 490–496.
- <sup>8</sup>Sharov, D. and Nakahashi, K., "A Boundary Recovery Algorithm for Delaunay Tetrahedral Meshing," *Proceedings of the 5<sup>th</sup> International Conference on Numerical Grid Generation in Computational Field Simulations*, 1996, pp. 229–238.
- <sup>9</sup>Kroo, I. M., "AA241 Course Notes," Stanford University, <http://adg.stanford.edu/aa241/AircraftDesign.html>.
- <sup>10</sup>Gordon, "Concorde SST," <http://concordesst.com>.
- <sup>11</sup>Liepmann, H. W. and Roshko, A., *Elements of Gasdynamics*, John Siley & Sons, 1957, pp. 109–113.

	Coordinates			Leading Wing			Following Wing		
	$x$	$y$	$z$	$C_L$	$C_D$	$L/D$	$C_L$	$C_D$	$L/D$
Case 1	1.0000	0.0000	-1.3416	0.14513	0.01839	7.89275	0.07111	0.01526	4.65900
Case 2	1.5000	0.0000	-1.3416	0.14508	0.01838	7.89319	0.14949	0.02155	6.93679
Case 3	2.0000	0.0000	-1.3416	0.14507	0.01838	7.89373	0.15884	0.01721	9.22928
Case 4	2.5000	0.0000	-1.3416	0.14513	0.01839	7.89164	0.13153	0.01786	7.36442
Case 5	1.5000	0.0000	-1.7889	0.14508	0.01839	7.88997	0.08472	0.01672	5.06691
Case 6	2.0000	0.0000	-1.7889	0.14511	0.01838	7.89617	0.15471	0.02118	7.30470
Case 7	2.5000	0.0000	-1.7889	0.14514	0.01838	7.89849	0.16161	0.01761	9.17680
Case 8	3.0000	0.0000	-1.7889	0.14492	0.01836	7.89220	0.13665	0.01802	7.58396
Case 9	1.0000	0.9487	-0.9487	0.14523	0.01840	7.89341	0.12154	0.01911	6.36079
Case 10	1.5000	0.9487	-0.9487	0.14505	0.01838	7.89243	0.15912	0.01990	7.99474
Case 11	2.0000	0.9487	-0.9487	0.14512	0.01838	7.89366	0.15363	0.01827	8.40758
Case 12	2.5000	0.9487	-0.9487	0.14509	0.01838	7.89453	0.14635	0.01815	8.06378
Case 13	1.5000	1.2649	-1.2649	0.14499	0.01837	7.89259	0.12995	0.01916	6.78285
Case 14	2.0000	1.2649	-1.2649	0.14521	0.01839	7.89572	0.15727	0.01972	7.97475
Case 15	2.5000	1.2649	-1.2649	0.14512	0.01838	7.89565	0.15432	0.01840	8.38756
Case 16	3.0000	1.2649	-1.2649	0.14520	0.01838	7.89943	0.14815	0.01826	8.11238
Case 17	0.5000	0.0000	1.3416	0.14508	0.01837	7.89768	0.14721	0.01833	8.03226
Case 18	1.0000	0.0000	1.3416	0.14516	0.01839	7.89514	0.14416	0.01895	7.60742
Case 19	1.5000	0.0000	1.3416	0.14533	0.01840	7.89899	0.09144	0.01728	5.29176
Case 20	2.0000	0.0000	1.3416	0.14512	0.01838	7.89539	0.10607	0.01268	8.36819
Case 21	2.5000	0.0000	1.3416	0.14514	0.01838	7.89538	0.15229	0.01891	8.05409
Case 22	1.0000	0.0000	1.7889	0.14519	0.01838	7.90058	0.14742	0.01835	8.03512
Case 23	1.5000	0.0000	1.7889	0.14493	0.01837	7.88755	0.14494	0.01890	7.66830
Case 24	2.0000	0.0000	1.7889	0.14513	0.01838	7.89390	0.10113	0.01754	5.76740
Case 25	2.5000	0.0000	1.7889	0.14504	0.01838	7.89340	0.11338	0.01361	8.32784
Case 26	3.0000	0.0000	1.7889	0.14520	0.01839	7.89621	0.15419	0.01892	8.15180
Case 27	1.0000	1.3416	0.0000	0.14517	0.01838	7.89766	0.16695	0.02041	8.17819
Case 28	1.5000	1.3416	0.0000	0.14507	0.01838	7.89084	0.16980	0.02001	8.48516
Case 29	2.0000	1.3416	0.0000	0.14506	0.01838	7.89319	0.17233	0.01954	8.82010
Case 30	1.5000	1.7889	0.0000	0.14512	0.01839	7.89160	0.15590	0.01967	7.92723
Case 31	2.0000	1.7889	0.0000	0.14500	0.01837	7.89267	0.15696	0.01927	8.14410
Case 32	2.5000	1.7889	0.0000	0.14508	0.01838	7.89225	0.15899	0.01881	8.45316
Case 33	3.0000	1.7889	0.0000	0.14506	0.01838	7.89287	0.15918	0.01893	8.40691
Case 34	0.9223	0.0000	-1.3962	0.14514	0.01839	7.89329	0.07249	0.01312	5.52443
Case 35	1.4215	0.0000	-1.4245	0.14510	0.01839	7.89011	0.12027	0.02043	5.88589
Case 36	1.9207	0.0000	-1.4529	0.14531	0.01839	7.90000	0.16766	0.01935	8.66560
Case 37	2.4199	0.0000	-1.4812	0.14498	0.01837	7.89042	0.14144	0.01676	8.43998
Case 38	1.3962	0.0000	-1.8710	0.14520	0.01839	7.89675	0.08333	0.01392	5.98501
Case 39	1.8954	0.0000	-1.8994	0.14519	0.01838	7.89706	0.12216	0.01991	6.13584
Case 40	2.3946	0.0000	-1.9277	0.14521	0.01839	7.89605	0.17006	0.02010	8.46122
Case 41	2.8938	0.0000	-1.9561	0.14536	0.01840	7.90053	0.14861	0.01705	8.71707
Case 42	1.4438	0.9487	-1.0322	0.14513	0.01839	7.89194	0.15355	0.02050	7.49049
Case 43	1.9430	0.9487	-1.0605	0.14513	0.01838	7.89672	0.15578	0.01841	8.46111
Case 44	2.4422	0.9487	-1.0889	0.14505	0.01837	7.89561	0.14764	0.01804	8.18517
Case 45	1.9251	1.2649	-1.3763	0.14520	0.01847	7.86282	0.15071	0.02010	7.49677
Case 46	2.4243	1.2649	-1.4046	0.14513	0.01839	7.89246	0.15659	0.01869	8.38013
Case 47	2.9235	1.2649	-1.4330	0.14499	0.01837	7.89129	0.15000	0.01817	8.25417
Case 48	0.5753	0.0000	1.3111	0.14512	0.01839	7.89052	0.14981	0.01834	8.16691
Case 49	1.0745	0.0000	1.2828	0.14520	0.01838	7.89800	0.13365	0.01914	6.98112
Case 50	1.5736	0.0000	1.2544	0.14524	0.01825	7.95987	0.07743	0.01494	5.18107
Case 51	2.0728	0.0000	1.2261	0.14518	0.01838	7.89699	0.14181	0.01367	10.37336
Case 52	2.5720	0.0000	1.1978	0.14522	0.01839	7.89708	0.14635	0.01952	7.49663
Case 53	1.0998	0.0000	1.7293	0.14529	0.01839	7.89974	0.15004	0.01837	8.16895
Case 54	1.5990	0.0000	1.7009	0.14531	0.01840	7.89729	0.13138	0.01906	6.89356
Case 55	2.0982	0.0000	1.6726	0.14529	0.01840	7.89833	0.08958	0.01499	5.97577
Case 56	2.5974	0.0000	1.6442	0.14531	0.01840	7.89939	0.13837	0.01516	9.12503
Case 57	3.0966	0.0000	1.6159	0.14504	0.01838	7.89282	0.14839	0.01938	7.65674
Case 58	1.4976	1.3416	-0.0850	0.14513	0.01839	7.89194	0.15355	0.02050	7.49049
Case 59	1.9968	1.3416	-0.1134	0.14513	0.01838	7.89672	0.15578	0.01841	8.46111
Case 60	2.4960	1.3416	-0.1417	0.14505	0.01837	7.89561	0.14764	0.01804	8.18517
Case 61	1.9968	1.7889	-0.1134	0.14520	0.01839	7.89664	0.15071	0.02010	7.49677
Case 62	2.4960	1.7889	-0.1417	0.14513	0.01839	7.89246	0.15659	0.01869	8.38013
Case 63	2.9952	1.7889	-0.1701	0.14499	0.01837	7.89129	0.15000	0.01817	8.25417

Table 1. Coordinates and aerodynamic performances of investigated formations